

# VolCCD: Fast Continuous Collision Culling between Deforming Volume Meshes

MIN TANG

Zhejiang University

DINESH MANOCHA

The University of North Carolina at Chapel Hill

SUNG-EUI YOON

KAIST

PENG DU

Zhejiang University

JAE-PIL HEO

KAIST

and

RUO-FENG TONG

Zhejiang University

111

We present a novel culling algorithm to perform fast and robust continuous collision detection between deforming volume meshes. This includes a continuous separating axis test that can conservatively check whether two volume meshes overlap during a given time interval. In addition, we present efficient methods to eliminate redundant elementary tests between the features (e.g., vertices, edges, and faces) of volume elements (e.g., tetrahedra, hexahedra, triangular prisms, etc.). Our approach is applicable to various de-

forming meshes, including those with changing topologies, and efficiently computes the first time of contact. We are able to perform inter-object and intra-object collision queries in models represented with tens of thousands of volume elements at interactive rates on a single CPU core. Moreover, we observe more than an order of magnitude performance improvement over prior methods.

Categories and Subject Descriptors: I.3.5 [Computer Graphics]: Computational Geometry and Object Modeling—*Physically based modeling*

General Terms: Algorithms

Additional Key Words and Phrases: Continuous collision detection, deforming volume meshes, continuous separating axis theorem, assignment culling

## ACM Reference Format:

Tang, M., Manocha, D., Yoon, S.-E., Du, P., Heo, J.-P., and Tong, R.-F. 2011. VolCCD: Fast continuous collision culling between deforming volume meshes. ACM Trans. Graph. 30, 5, Article 111 (October 2011), 15 pages.  
DOI = 10.1145/2019627.2019630  
<http://doi.acm.org/10.1145/2019627.2019630>

This research is supported in part by National Basic Research Program of China (No. 2011CB302205), ARO Contract W911NF-10-1-0506, and NSF awards 0917040, 0904990, and 1000579. M. Tang is supported in part by Natural Science Foundation of China (No. 60803054, 61170140), Natural Science Foundation of Zhejiang, China (No. Y1100069), Important Science and Technology Specific Project of Zhejiang, China (2008C01059-4). S. Yoon is supported in part by MKE/MCST/IITA [2008-F-033-02], KRF-2008-313-D00922, KMCC, MSRA, BK, DAPA/ADD (UD080042AD), MKE/KEIT [K1001810035261], MEST/NRF/WCU (R31-2010-000-30007-0), and VFX simulation techniques.

Authors' addresses: M. Tang (corresponding author), Zhejiang University, China; email: tang\_m@zju.edu.cn; D. Manocha, The University of North Carolina at Chapel Hill; S.-E. Yoon, KAIST, South Korea; P. Du, Zhejiang University, China; J.-P. Heo, KAIST, South Korea; R.-F. Tong, Zhejiang University, China.

Permission to make digital or hard copies of part or all of this work for personal or classroom use is granted without fee provided that copies are not made or distributed for profit or commercial advantage and that copies show this notice on the first page or initial screen of a display along with the full citation. Copyrights for components of this work owned by others than ACM must be honored. Abstracting with credit is permitted. To copy otherwise, to republish, to post on servers, to redistribute to lists, or to use any component of this work in other works requires prior specific permission and/or a fee. Permissions may be requested from Publications Dept., ACM, Inc., 2 Penn Plaza, Suite 701, New York, NY 10121-0701 USA, fax +1 (212) 869-0481, or permissions@acm.org.

© 2011 ACM 0730-0301/2011/10-ART111 \$10.00

DOI 10.1145/2019627.2019630

<http://doi.acm.org/10.1145/2019627.2019630>

## 1. INTRODUCTION

Many physically-based simulation algorithms use volume meshes to represent deformable objects. Volume meshes (e.g., tetrahedral meshes) are a polygonal representation of the interior volume of an object and correspond to a discrete representation of the internal structure of the object. Such regular or irregular grids are commonly used in finite element analysis and other Lagrangian mesh-based simulation algorithms.

In this article, we address the problem of fast and reliable collision detection between volume meshes (see Figure 1). As forces are applied, the objects deform, and the nodes or points inside the object move. Our goal is to compute all the contacts between deforming volume meshes, including self-collisions. In order to perform reliable collision checking, we focus mainly on *Continuous Collision Detection* (CCD) [Provot 1997; Bridson et al. 2002; Redon et al. 2002]. The CCD algorithms typically perform linear interpolation

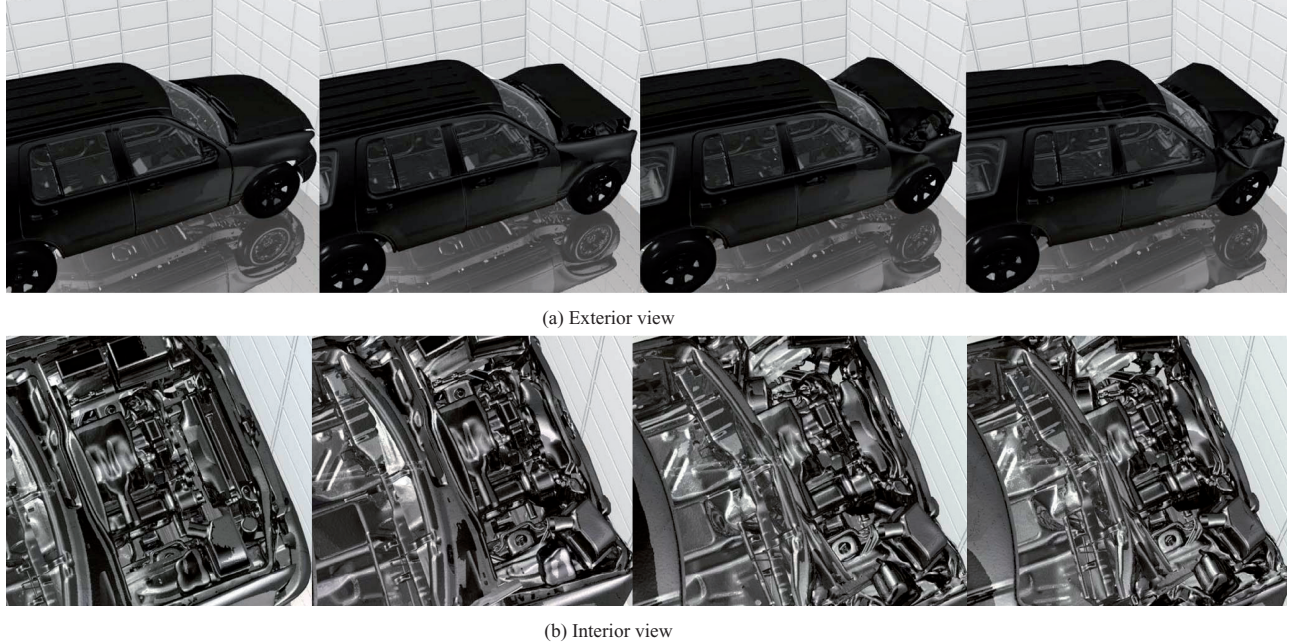


Fig. 1. Car crash: A Ford Explorer with 1.2M shell elements crashes against a rigid wall and deforms. The underlying finite-element simulation is performed using LS-DYNA package for crash analysis, which performs contact computations between the shell elements. These figures show exterior and interior views during the crash simulation. Average CCD query time for both inter- and intracollision detection using VolCCD is 3.3 seconds per frame on a single core of 2.4 GHz Intel Q6600 CPU. We obtain 12 times performance improvement over prior collision detection algorithms for this benchmark.

between discrete vertex positions of the volume meshes and check for collisions among swept volumes by performing elementary tests. These CCD methods provide accurate and robust collision results by computing the first time of contact, preventing interpenetrations, and detecting collisions even between fast moving objects.

Volume meshes and FEM methods are increasingly used in interactive applications such as games and surgical simulators. These include simulating solid or soft-tissue deformations, fracturing, suturing, cutting, etc. In many applications, it is also important to compute all the contacts among external and internal elements of volume meshes for a high-quality simulation [LS-DYNA 2001; O'Brien 2000]. However, it is a major challenge to perform interactive and reliable collision queries in these simulations [Irving et al. 2004; Teschner et al. 2005; Parker and O'Brien 2009; Zhu et al. 2010].

Most of the prior work on CCD algorithms, unfortunately, has been limited to surface meshes represented as triangulated models and thus check for collisions only at the boundaries of the objects. Furthermore, these methods do not work well when the simulation results in topological changes (e.g., fracturing) on the surface meshes [Heo et al. 2010]. Moreover, current techniques for collision checking between volume meshes mainly perform discrete collision checking at fixed time steps using spatial subdivisions, distance fields, or image-space techniques. Since these discrete methods can miss collisions, especially when objects deform drastically or move fast, many simulation techniques with volume meshes typically use rather small time steps and thus run very slowly.

**Main results.** We present novel algorithms for fast CCD computation between volume meshes. Our approach can handle all regular or irregular meshes, where each volumetric element is a convex polytope. Moreover, the approach is general and makes no assumptions about motion, deformation, or topology.

We describe two new culling methods, feature-level and element-level culling techniques, to accelerate the computation. The first culling technique is based on continuous separating axis tests between the features (e.g., vertices, edges, and faces) and volumetric elements (e.g., tetrahedra, hexahedra, triangular prisms, etc.). Our formulation uses separating axes to conservatively check whether there is a collision between two volume meshes during a given time interval (see Section 4). This test is simple and robust, since it reduces to performing a small number of dot products. In addition, we present techniques to eliminate redundant elementary tests between the features by exploiting mesh connectivity (see Section 5). In particular, we use a feature-level assignment culling that can also handle changes in the mesh connectivity.

The overall CCD algorithm uses a k-DOP hierarchy and can perform interobject as well as intraobject collisions. The combination of separating axis tests and feature-level culling can significantly improve the culling efficiency (see Section 6).

We highlight the performance of our CCD algorithm on volume meshes arising from various engineering, medical, and animation simulations with a few thousand to hundreds of thousands of tetrahedra or triangular prisms. In practice, our algorithm can reliably check for collisions in tens to hundreds of milliseconds on a single 2.4 GHz core. We observe up to two orders of magnitude reduction in the number of elementary tests and more than an order of magnitude performance improvement over prior methods (see Section 6). Moreover, we are able to produce realistic simulation results (e.g., fracturing) over collision methods that check collisions only at the boundary at discrete time steps.

**Organization.** The rest of the article is organized in the following manner. We survey some related work in Section 2 and give an overview of our approach in Section 3. Section 4 describes our novel culling scheme based on separating axis test. We present the feature-level culling method in Section 5 and highlight the performance in

Section 6. We analyze the approach and compare with prior methods in Section 7.

## 2. RELATED WORK

The problem of collision detection between deformable models has been well studied. We refer the reader to a recent survey on collision detection algorithms [Teschner et al. 2005] and physically-based deformable models [Nealen et al. 2006]. At a broad level, prior methods for collision queries can be classified as surface-based and volume-based methods.

### 2.1 Collision Queries on Polygonal Models

Most prior techniques have been designed for triangulated models and check for collisions only at the boundary (or surface) of the objects. The simplest algorithms compute bounding volume hierarchies and update the hierarchies using refitting or rebuilding algorithms as the objects deform [Teschner et al. 2005].

CCD provides more accurate collision results than Discrete Collision Detection (DCD). Therefore, CCD has been studied relatively recently for rigid models [Redon et al. 2002], articulated models [Zhang et al. 2007], and deformable models [Provot 1997; Bridson et al. 2002; Govindaraju et al. 2005]. Since CCD requires longer computation time than DCD, different acceleration techniques have been proposed. Some of them are based on normal cone culling [Tang et al. 2009], removing redundant elementary tests [Hutter and Fuhrmann 2007; Curtis et al. 2008], and coplanarity-based culling [Tang et al. 2010a]. The elementary tests between the primitives (e.g., triangles) are performed using polynomial root solvers [Provot 1997] or local advancement methods [Tang et al. 2010b].

### 2.2 Collision Queries for Volume Meshes

Current techniques for collision checking on volume meshes are mainly limited to discrete collision queries, where they check for contacts at specific time steps. Teschner et al. [2003] presented a spatial subdivision method to efficiently perform collision checking for tetrahedral meshes and integrated it with different FEM-based simulation systems [Heidelberger et al. 2004]. Mathias and Gu [2007] extended this approach for real-time applications. O'Brien [2000] and Müller et al. [2001] check for collisions between the volume elements using Bounding Volume Hierarchies (BVHs) for fracture simulations. Distance field methods are widely used to check for contacts and penetrations [Sud et al. 2006] and have been applied to volume meshes [Fisher and Lin 2001; Heidelberger et al. 2004; Teschner et al. 2005; Wojtan et al. 2009] to perform queries at a given distance field resolution. Other methods use the rasterization hardware to perform interactive queries at image-space resolution between volume meshes [Lombardo et al. 1999; Heidelberger et al. 2003; Faure et al. 2008; Allard et al. 2010]. However, most of these methods perform discrete collision checking at a specific time instance, as opposed to CCD between volume meshes. Therefore, simulations that employ these discrete methods can miss collisions and thus use small time steps to reduce the chance of missing collisions.

## 3. OVERVIEW

In this section, we introduce the notation used in the rest of the article and give an overview of our approach.

### 3.1 Notation and Definitions

Many deformable and FEM simulations use volumetric elements such as tetrahedra, hexahedra, and triangular prisms to represent the interior volume of objects. We use the symbols of  $V$ ,  $E$ ,  $F$ , and  $O$  to represent the vertices, edges, faces, and volumetric elements of an object, respectively. The lower-case symbols of  $v$ ,  $e$ ,  $f$ , and  $o$  denote a specific vertex, edge, face, and volumetric element, respectively. We define a volumetric element as a simple polytope consisting of  $n_v$  vertices,  $n_e$  edges, and  $n_f$  triangles. We also use the term of deforming volume meshes for models defined by these volumetric elements. The operators “ $*$ ”, “ $\cdot$ ”, and “ $\times$ ” denote the product of two scalar values (or a scalar value and a vector), the dot product of two vectors, and the cross product of two vectors, respectively.

Our algorithm does not make any assumption about the motion or the underlying deformation or the topology of the object. The inputs for our algorithm are the initial and final positions of each vertex corresponding to two discrete time instances. We denote the time interval as  $[0, 1]$ . Similar to prior surface-based CCD algorithms [Provot 1997; Bridson et al. 2002], we assume that the motion of each vertex of the volume mesh can be represented by a constant velocity between the two time steps; we also briefly discuss how our approach can be extended to handle nonconstant velocities. Our goal is to check for collisions between all the deforming volumetric elements of the same object (i.e., intra-object collisions) and different objects (i.e., inter-object collisions) during the time interval and compute the first time of contact.

### 3.2 Collision Checking between Volume Meshes

Most prior work in collision detection can be broadly classified as Discrete Collision Detection (DCD) or CCD methods. In general, CCD methods tend to be more expensive, as they check for collisions along the entire trajectory. However, the CCD methods are more accurate and can guarantee that no collision is missed between the discrete time steps. This makes it possible to employ large time steps during the simulation. On the other hand, simulation algorithms based on DCD tend to choose smaller time steps [Parker and O'Brien 2009], in order to reduce the chances of missing collisions and thus maintain the fidelity of the simulation. However, using a small simulation time step can slow down the overall performance of the simulation. Most of the earlier work in collision detection was based on DCD algorithms. CCD techniques have been shown recently to be useful to perform robust collision detection and handling for many applications [Provot 1997; Redon et al. 2002; Bridson et al. 2002].

One may consider that identifying collisions among the internal elements based on the CCD framework may be unnecessary, since surface-based CCD methods can accurately compute the first time of contact at the boundary. However, contacts can occur even among internal elements, especially under strong external forces or high impacts with fast moving objects. Even though the surface-based CCD methods can identify the first time of contact and the associated boundary features, current contact resolution methods may not be able to accurately resolve those contacts and may result in interpenetrations during subsequent frames of the simulation [Volino and Magnenat-Thalmann 2006]. In this case, it is important to identify all the collisions between the internal elements and resolve them in an appropriate manner.

Many of existing physically-based simulation algorithms check only for collisions at the surface boundary. However, for many CAD/CAM and virtual prototyping applications, such as crash simulation or structure analysis, it is important to check the features of

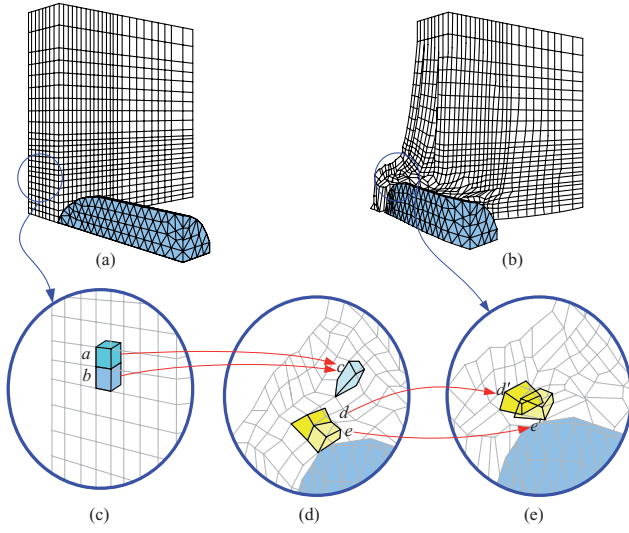


Fig. 2. Topological changes: When a high-speed bullet hits a metal plate, topological changes occur (e.g., elements  $a$  and  $b$  merge into  $c$ , and the connectivity of the elements  $d$  and  $e$  changes). These kinds of simulations with such topological changes can result in a high number of collisions and penetrations among the interior elements of volume meshes. Our algorithm can compute the first time-of-contact among the elements in an efficient manner.

interior volume elements for collisions [Hallquist 2006; ABAQUS 2003]. Therefore, these FEM systems perform various kinds of contact and penetration computations [LS-DYNA 2001], and these contact computations can take a significant fraction of the overall simulation time.

In some applications, such as fluid simulation [Fleissner et al. 2007; Plimpton et al. 1998], there are no explicit boundary elements. Such fluid simulations or other complex simulations often undergo topological changes such as explosions or penetrations shown in Figure 2, or cracks [Sifakis et al. 2007]. As a result, the connectivity between the boundary and interior elements changes. It is required to check for collisions among all those elements for realistic simulation. If there is a severe deformation due to a large external force in simulations, it can result in complex topological changes. This is illustrated in Figure 2.

We give a broad overview of finite-element simulation that checks for collisions between the internal volume elements (Algorithm 1). The overall simulation framework is similar to the ones described in Müller et al. [2001], O'Brien [2000], and O'Brien and Hodgins [1999]. All the volumetric elements in the scene are organized in a hierarchical manner using a BVH. Volume-based collision checking is performed by traversing the BVH in top-down manner and searching all the contacts [O'Brien 2000]. Next, the impact forces are calculated based on these contacts and the nodes are updated with the accumulated forces (internal forces, external forces, etc.). For the nodes undergoing forces that exceed their failure stresses or the merging thresholds, the topology structures around them are updated with splitting and gluing operations [Müller et al. 2001; O'Brien and Hodgins 1999; Wojtan et al. 2009]. Otherwise the nodes are updated based on Newton's second law.

In the example shown in Figure 2, we show that at the end of a specific simulation time step, two volumetric elements  $a$  and  $b$  merge into  $c$  due to the impact force (lines 28–33 of Algorithm 1). Also, two adjacent elements  $d$  and  $e$  break their connectivity and

---

**ALGORITHM 1:** FEM simulation with volume-based collision detection:

---

```

1: // Stage 1: Preprocessing.
2: Build BVH  $B$  for the whole scene.
3:
4: // Stage 2: Solving iteratively.
5:  $t = t_0$ 
6: while  $t <= t_1$  do
7:   for all volumetric elements  $o_i \in$  the set of elements  $elm$  do
8:     Calculate internal forces  $f_j^i$  at each nodes  $nd_j$ .
9:     Calculate external forces  $f_j^e$  at each nodes  $nd_j$ .
10:    // Check volumetric elements for contacts.
11:    if Any contact detected then
12:      Compute contact information  $\{t', d_j\}$ .
13:      // Here  $t' \in [t, t + \Delta t]$  is the first-time-of-contact,
14:      // and  $d_j$  is the penetration depth.
15:      // Calculate impact forces  $f_j^m$  of each nodes  $nd_j$ ,
16:      // based on the contact information  $\{t', d_j\}$ , i.e.,
17:       $f_j^m = ImpactForce(nd_j, \{t', d_j\})$ 
18:    else
19:       $f_j^m = 0$ 
20:    end if
21:  end for
22:
23:  for all nodes  $nd_j \in$  the set of nodes  $nds$  do
24:    // Update position of each node  $nd_j$  based on
25:    // accumulated forces  $f_j^i + f_j^e + f_j^m$ , i.e.,
26:     $f_j^a = f_j^i + f_j^e + f_j^m$ 
27:    // Checking for merging threshold.
28:    for all nodes  $nd_k$  in the near proximity of  $nd_j$  do
29:      if  $f_j^a > merging\_threshold_{jk}$  then
30:        Merge  $nd_j$  and  $nd_k$  into a new node  $nd_l$ ,
31:        and adjust position of  $nd_l$  accordingly.
32:      end if
33:    end for
34:    // Checking for failure stress.
35:    if  $f_j^a > failure\_stress_j$  then
36:      Split  $nd_j$  into two new nodes  $nd_p$  and  $nd_q$ ,
37:      and adjust the positions of  $nd_p$  and  $nd_q$  accordingly.
38:    end if
39:    if No topology change then
40:       $pos_j^{t+\Delta t} = UpdatePosition(pos_j^t, f_j^a)$ 
41:    end if
42:  end for
43:
44:  Update the BVH  $B$ .
45:   $t = t + \Delta t$ 
46: end while
47:
48: // Stage 3: Output simulation result.
49: Output results.

```

---

penetrate with each other (lines 35–38 of Algorithm 1). This kind of topological change results in collisions between the interior features of a mesh. Therefore, we can get deeper interpenetrations among internal elements of models.

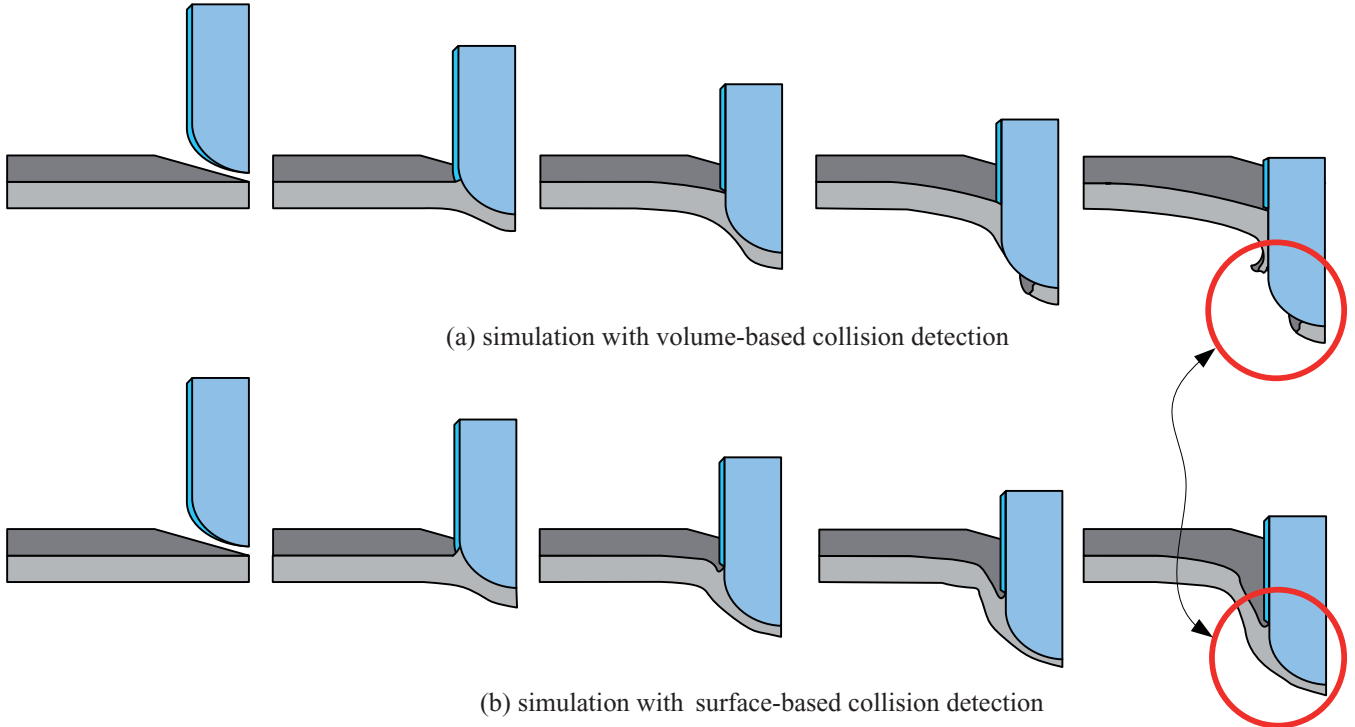


Fig. 3. Comparison between surface-based and volume-based collision detection: These two figures show two simulation sequences of a bullet penetration benchmark generated with volume-based collision detection (a) and surface-based collision detection (b). In this simulation, a bullet hits a steel plate. Since the steel plate is thin, the plate should fracture given the high-speed bullet. The highlighted areas stress the difference between the simulation results. For this benchmark, checking collisions between the interior features is essential to compute the interior impact forces that result in cracks and fractures, and thereby generate an accurate simulation. For these simulation results, we use LS-DYNA.

Figure 3 highlights the benefit of performing collision checking between volume elements on the bullet penetration benchmark. In Figure 3(b), we show simulation results achieved by checking for collisions only at the boundary (i.e., only the boundary features). In Figure 3(a), we show the result achieved also by taking into account collision checking between the internal volume elements (i.e., boundary + interior features). The highlighted areas stress the difference between the simulation results. For this benchmark, checking collisions between interior features is essential both to reflect interior impact forces producing fractures and to generate accurate simulation results.

### 3.3 Acceleration Using Bounding Volume Hierarchies

We use a k-DOP bounding volume hierarchy to accelerate the computation. The hierarchy is used to cull away pairs of volumetric elements that are not in close proximity. A k-DOP (specifically a 16-DOP in our system) hierarchy  $B$  is computed for all the volumetric elements in the scene and updated as the objects move or deform. The 16-DOPs are constructed similar to the 18-DOPs as described in Klosowski et al. [1998]. The reasons that we use 16-DOPs are twofold: (1) it provides a higher culling ratio over other simple bounding volumes such as axis-aligned bounding box and (2) it can be updated efficiently. For example, the computation can be accelerated with SIMD instructions (e.g., SSE instructions on current CPUs). Furthermore, we use restructuring and refitting algorithms to update the k-DOP hierarchy for deforming volume meshes in an efficient manner. In our benchmarks, updating a

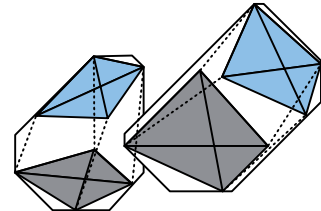


Fig. 4. Bounding volumes of volumetric elements: We use tight-fitting k-DOPs to enclose the swept volume of each deforming volumetric element. In practice, these k-DOPs can result in a high number of false positives.

k-DOP-based BVH takes a minor portion, about 2.45% to 7.56%, of the total query time.

Each leaf node of  $B$  encloses the volume swept by a single element  $o$  that is deforming during the time interval  $[0, 1]$ . Collision detection is performed by traversing  $B$  recursively in a top-down manner and checking the bounding volumes for overlap. For every overlapping pair of leaf nodes, exact collision checking between the volumetric elements is performed by using elementary tests. In practice, the number of overlapping bounding boxes tends to be rather high for deforming meshes and may result in a very high number of false positives (Figure 4).

### 3.4 CCD between Volumetric Elements

Let us assume that a given pair of volumetric elements does not overlap at  $t = 0$ ; we will discuss how our method behaves when there are overlaps at the initial position. In that case, the first time of contact between these (internal or external) volumetric elements occurs at the boundary features, corresponding to the vertices, edges, or faces. Prior work on CCD computation has been limited to triangle primitives and performs 15 elementary tests: 9 Edge-Edge (EE) and 6 Vertex-Face (VF) tests [Provot 1997; Bridson et al. 2002]. Each elementary test reduces to finding roots of a cubic polynomial.

This formulation can be extended to volumetric elements. Suppose that we have two volumetric elements,  $o^i$  and  $o^j$ ;  $o^i$  has  $n_v^i$  vertices,  $n_e^i$  edges, and  $n_f^i$  triangles, and  $o^j$  has  $n_v^j$  vertices,  $n_e^j$  edges, and  $n_f^j$  triangles. In the case that  $o^i$  and  $o^j$  are not adjacent, that is, do not share any boundary elements between them, computing the first time of contact reduces to performing  $(n_v^i * n_f^j + n_v^j * n_f^i)$  VF elementary tests and  $n_e^i * n_e^j$  EE tests. For example, a primitive test for two tetrahedra requires to perform 32 VF and 36 EE tests. Similarly, a primitive test for two hexahedra requires performing 192 VF and 144 EE elementary tests (see Figure 4).

### 3.5 Our Approach

The problem of performing CCD tests between volume meshes is considerably more expensive and complicated than handling surface meshes. This is due to the following reasons.

- (1) Bounding volumes of the leaf nodes of a BVH  $B$  tend to be more conservative since those bounding volumes enclose the swept volumetric elements in the time interval  $[0, 1]$ . As a result, the number of false positives given the CCD using a BVH is very high (e.g., 90% ~ 99% in our benchmarks).
- (2) The cost of an exact CCD between volume meshes is much higher, for example, 4 – 20 times more expensive as compared to CCD between triangles, because of the higher number of elementary tests.
- (3) Culling methods based on normal cones or bounds [Volino and Thalmann 1994; Provot 1997; Tang et al. 2009; Heo et al. 2010] are designed originally for detecting self-collision free regions of surface meshes. These techniques cannot be applied to volume meshes, since it is unclear how to compute normals for internal elements of volume meshes.

In order to accelerate the computation, we present two new culling techniques to reduce the number of false positives and remove redundant elementary tests. These methods are applied to the volumetric elements as elementary-level culling, and to features of each element as feature-level culling. This includes a *Continuous Separating Axis Theorem* (CSAT) that can significantly reduce the number of false positives between the volumetric elements. Moreover, we present a feature-level *assignment culling* scheme that is used to remove all duplicate or redundant elementary tests between pairs of volumetric elements.

During each simulation time step, our CCD algorithm proceeds in three stages. The overall pipeline of the CCD algorithm is shown in Figure 5. At the first stage, we perform bounding volume traversal and cull away nonoverlapping pairs. We also apply CSAT to the leaf node pairs to reduce the false positives. At the second stage, we perform feature-level culling that handles nonadjacent and adjacent volumetric elements in separate steps. For nonadjacent volumetric element pairs, assignment culling is used to remove redundant elementary tests. Moreover, we present the notion of *O-Set pairs*,

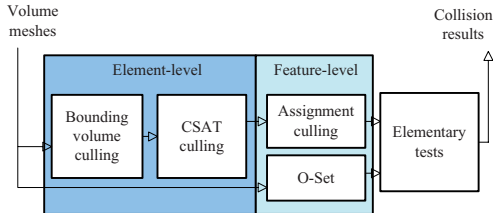


Fig. 5. CCD algorithm for deforming volume meshes: By performing element-level and feature-level culling, we drastically reduce the number of false positives and achieve interactive CCD performance on complex volumetric benchmarks.

which refers to the minimal number of elementary tests between adjacent pairs that are not classified as parts of the tests between the nonadjacent pairs, and can be easily recomputed to handle topological changes. At the third, final stage, exact elementary tests are preformed.

## 4. CSAT CULLING ALGORITHM

In this section, we present our culling algorithm based on the Continuous Separating Axis Theorem (CSAT). The objective is to derive sufficient conditions for nonoverlap elements during the  $[0, 1]$  time interval. We first present the CSAT formulation for two vertices undergoing continuous motion during the  $[0, 1]$  time interval. Next, we extend it to perform VF and EE tests, and finally to the volumetric elements.

### 4.1 Continuous Separating Axis Theorem

Given two convex shapes, the Separating Axis Theorem (SAT) states that if there exists a line onto which the projections of two objects do not overlap, then the objects do not intersect. The resulting line with disjointed projections is called the *separating axis*. Separating axis tests are widely used for fast overlap tests between oriented bounding boxes [Gottschalk et al. 1996] and convex shapes. Eberly [2000] extended the SAT formulation to perform overlap tests between rigid convex polytopes that are moving with constant linear velocity and no angular velocity.

We extend SAT designed for rigid convex polytopes to continuous tests between deforming volumetric elements, whose vertices have a constant velocity. Our formulation is conservative, and provides sufficient conditions for nonoverlapping during the given time interval. Furthermore, we show that the resulting CSAT between two volume elements can be performed efficiently by a few dot products.

**THEOREM 1 (CSAT FOR TWO MOVING VERTICES).** *Suppose two moving vertices  $p$  and  $q$ , defined by their positions at the time interval  $[0, 1]$  ( $p_0$  and  $p_1$  and  $q_0$  and  $q_1$ , respectively), and a separating axis defined by  $\mathbf{L} (\neq 0)$ . If  $(q_0 - p_0) \cdot \mathbf{L}$  and  $(q_1 - p_1) \cdot \mathbf{L}$  have the same sign,  $q$  will not overlap with  $p$  during the time interval.*

Due to the page limit, we provide proofs of this theorem and other corollaries in the Appendix.

Overall, this theorem provides a simple, sufficient condition when two vertices moving along the straight lines have no collisions during the given time interval (as shown in Figure 6(a)). In Section 4.4, we extend this theorem to perform overlap tests between two volumetric elements.

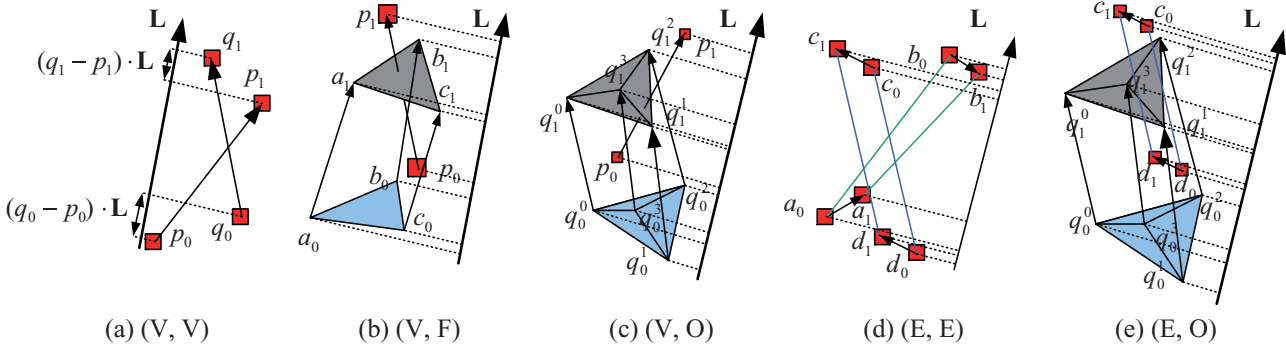


Fig. 6. CSAT culling algorithm: the Continuous Separating Axis Theorem (CSAT) culling methods (a) for two moving vertices, (b) for a VF test between a vertex and a triangle, (c) for VF tests between a vertex and a volumetric element, (d) for a EE test between two edges, and (e) for EE tests between an edge and a volumetric element. For each case shown in (b) – (e), we can conclude that these deforming features/elements do not overlap with each other during the time interval based on CSAT tests.

## 4.2 VF Pairs

Based on the CSAT for two moving vertices, we derive the following culling test for a VF pair.

**COROLLARY 1 (CSAT BETWEEN A VERTEX AND A TRIANGLE).** Suppose a vertex  $p$  and a triangle  $f$  defined by their positions at the time interval  $[0, 1]$  ( $p_0$  and  $p_1$  for  $p$ , and  $a_0, b_0, c_0$  and  $a_1, b_1, c_1$  for  $f$ , respectively), and a vector  $\mathbf{L}$  ( $\neq 0$ ). If the following 6 expressions have the same sign:

$$(a_0 - p_0) \cdot \mathbf{L}, \quad (a_1 - p_1) \cdot \mathbf{L}, \quad (b_0 - p_0) \cdot \mathbf{L}, \quad (b_1 - p_1) \cdot \mathbf{L}, \quad (c_0 - p_0) \cdot \mathbf{L}, \quad (c_1 - p_1) \cdot \mathbf{L}, \quad (1)$$

then  $p$  and  $f$  will not overlap during the time interval.

This culling condition implies if the projection of a vertex  $p$  is above/below all the projections of the three corners of a triangle  $f$  at  $t = 0$  and  $t = 1$ , then  $p$  and  $f$  will not overlap during the interval (as shown in Figure 6(b)). The choice of  $\mathbf{L}$  is important in terms of performance. In practice, we use the initial normal vector of  $f$ ,  $\mathbf{n}_0$ , as the projection axis. In such case,  $(a_0 - p_0) \cdot \mathbf{n}_0 = (b_0 - p_0) \cdot \mathbf{n}_0 = (c_0 - p_0) \cdot \mathbf{n}_0$ , so we need to perform only 4 dot products for this culling test.

**COROLLARY 2 (CSAT BETWEEN A VERTEX AND A VOLUMETRIC ELEMENT).** Suppose a vertex  $p$  and a volumetric element  $o$  (with  $n_v$  vertices and  $n_f$  triangles) defined by their positions during the time interval  $[0, 1]$  ( $p_0$  and  $p_1$  for  $p$ , and  $q_0^i$  and  $q_1^i$  for  $o$ ,  $i \in [0, n_v - 1]$ ), and a vector  $\mathbf{L}$  ( $\neq 0$ ). If the following  $2 * n_v$  algebraic expressions have the same sign:

$$(q_0^i - p_0) \cdot \mathbf{L}, \quad i \in [0, n_v - 1], \quad (2)$$

$$(q_1^i - p_1) \cdot \mathbf{L}, \quad i \in [0, n_v - 1],$$

then  $p$  and all the  $n_f$  triangles of  $o$  will not overlap during the time interval.

This culling condition provides a simple nonoverlapping condition between the moving vertex and the volume swept by  $o$ . We randomly pick a face from the volumetric element, and use  $n_0$  of the face as  $\mathbf{L}$ . For a tetrahedron ( $n_v = 4$  and  $n_f = 4$ ), we need to perform only 8 dot products for this test (as shown in Figure 6(c)).

## 4.3 EE Pairs

**COROLLARY 3 (CSAT BETWEEN TWO EDGES).** Suppose two edges,  $e^1$  and  $e^2$ , defined by their end positions during  $t \in [0, 1]$  ( $a_0, b_0$  and  $a_1, b_1$  for  $e^1$ , and  $c_0, d_0$  and  $c_1, d_1$  for  $e^2$ ), and a vector  $\mathbf{L}$  ( $\neq 0$ ). If the following eight expressions have the same sign:

$$(a_0 - c_0) \cdot \mathbf{L}, (a_1 - c_1) \cdot \mathbf{L}, (b_0 - c_0) \cdot \mathbf{L}, (b_1 - c_1) \cdot \mathbf{L}, \quad (3)$$

$$(a_0 - d_0) \cdot \mathbf{L}, (a_1 - d_1) \cdot \mathbf{L}, (b_0 - d_0) \cdot \mathbf{L}, (b_1 - d_1) \cdot \mathbf{L},$$

then  $e^1$  and  $e^2$  do not overlap during the time interval.

This implies that if the projections of the two end points of an edge  $e^1$  are above/below the projections of the two end points of another edge  $e^2$  at  $t = 0$  and  $t = 1$ , then  $e^1$  and  $e^2$  will not overlap during the time interval (as shown in Figure 6(d)). All these tests can be performed by using 8 dot products. Again, the choice of  $\mathbf{L}$  is important in terms of performance. In practice, we use  $\mathbf{n}_0 = (a_0 - b_0) \times (c_0 - d_0)$ , as the projection axis. In such a case,  $(a_0 - c_0) \cdot \mathbf{n}_0 = (b_0 - c_0) \cdot \mathbf{n}_0 = (a_0 - d_0) \cdot \mathbf{n}_0 = (b_0 - d_0) \cdot \mathbf{n}_0$ , so we only need to perform 5 dot products to perform this culling method.

**COROLLARY 4 (CSAT BETWEEN AN EDGE AND A VOLUMETRIC ELEMENT).** Suppose an edge  $e$  and a volumetric element  $o$  (with  $n_v$  vertices and  $n_e$  edges) defined by their positions at time interval  $[0, 1]$  ( $c_0$  and  $c_1$  and  $d_0$  and  $d_1$  for  $e$ , and  $q_0^i$  and  $q_1^i$  for  $o$ ,  $i \in [0, n_v - 1]$ ), and a vector  $\mathbf{L}$  ( $\neq 0$ ). If the following  $4 * n_v$  expressions have the same sign:

$$(q_0^i - c_0) \cdot \mathbf{L}, \quad i \in [0, n_v - 1], \quad (q_1^i - c_1) \cdot \mathbf{L}, \quad i \in [0, n_v - 1], \quad (4)$$

$$(q_0^i - d_0) \cdot \mathbf{L}, \quad i \in [0, n_v - 1], \quad (q_1^i - d_1) \cdot \mathbf{L}, \quad i \in [0, n_v - 1],$$

then  $e$  and  $o$  do not overlap during the time interval.

We randomly pick an edge from the volumetric element and use  $\mathbf{n}_0 = (a_0 - b_0) \times (c_0 - d_0)$  as the choice of  $\mathbf{L}$ . For a tetrahedron ( $n_v = 4$  and  $n_e = 6$ ), we need to evaluate only 16 dot products by using this culling method.

## 4.4 CSAT between Volumetric Elements

Let the two volumetric elements be:  $o^i$  with  $n_v^i$  vertices,  $n_e^i$  edges, and  $n_f^i$  triangles, and  $o^j$  with  $n_v^j$  vertices,  $n_e^j$  edges, and  $n_f^j$  triangles. In the case that  $o^i$  and  $o^j$  are not adjacent, that is, do not share



Fig. 7. Octopi benchmark: Three deforming octopi with 24 tentacles consist of 17.6K tetrahedra. The simulation has multiple inter-object and intra-object collisions. The average CCD query time is 75ms per frame.

any boundary elements between them, we can compute the first time of contact between  $o^i$  and  $o^j$  by performing VF tests between the vertices of one element and the faces of another element, and by performing EE tests between the edges of those two elements. Therefore, we have to perform  $(n_v^i * n_f^j + n_v^j * n_f^i)$  VF tests and  $n_e^i * n_e^j$  EE tests.

Note that our culling method that uses the CSAT between a vertex and an element requires  $2 * n_v$  dot products, where  $n_v$  is the number of vertices of the element. Therefore, all the VF tests with our CSAT culling method need to perform  $4 * n_v^i * n_v^j (= 2 * n_v^i * n_v^j + 2 * n_v^j * n_v^i)$  dot products. Also, our culling method that uses the CSAT between an edge and an element performs  $4 * n_v$  dot products. As a result, all the EE tests between two volumetric elements can be performed with our CSAT culling method using  $4 * n_e^i * n_e^j$  or  $4 * n_e^j * n_e^i$  dot products. A detailed pseudocode description of CSAT culling between two volumetric elements is given in Algorithm 2 of the Appendix.

*Separating axis, L.* Depending on the chosen L, the performance of our culling method varies. In our benchmarks, the chosen L provides a high culling efficiency that reduces the number of operations. Other alternatives, such as selecting L from predetermined features or predicting L by overall velocities of volumetric elements, are possible. However, we found that they do not improve the performance in our experiments.

## 5. FEATURE-LEVEL CULLING

Models represented by volume meshes tend to result in a high number of intra-object collisions. These include overlap tests between adjacent volumetric elements and nonadjacent volumetric elements. After applying CSAT culling, the overall algorithm performs elementary tests between the features of the volumes to compute the first time of contact.

In this section, we present two culling techniques that can eliminate any duplicate or redundant elementary tests. We present two methods: *O-Sets* for adjacent volumetric elements and *assignment culling* for nonadjacent volumetric elements. We have to perform elementary tests with features of all the volumetric elements that pass CSAT culling. However, we drastically reduce the number of tested elementary tests based on the O-Sets and assignment culling. Furthermore, we show how these techniques can also handle topological changes in the volume meshes.

### 5.1 O-Sets

The CCD tests between the volumetric elements are performed independently. In terms of handling two adjacent volumetric ele-

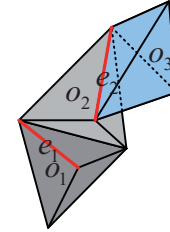


Fig. 8. Duplicate EE tests between adjacent volumetric elements: an EE test  $\{e_1, e_2\}$  between an adjacent pair  $\{o_2, o_3\}$  is covered by the tests of a nonadjacent pair  $\{o_1, o_3\}$  by using O-Sets.

ments, the number of elementary tests turns out to be less than  $n_v^i + n_v^j + n_v^i * n_f^j$  VF tests and  $n_e^i * n_e^j$  EE tests, because some of the features are shared. Moreover, the algorithm can be proceeded in a more efficient manner by checking the nonadjacent volumetric pairs for overlap first, followed by adjacent volumetric pairs. We extend the orphan set idea proposed for surface meshes [Tang et al. 2009] to the O-Sets for volume elements and compute the minimal number of elementary tests that need to be performed between adjacent volume meshes.

In order to explain the O-Set, consider the example shown in Figure 8. Some of the EE tests (e.g.,  $\{e_1, e_2\}$ ) corresponding to adjacent elements are same as the EE tests that need to be tested for collisions among the nonadjacent elements. We define the O-Set to be the feature pairs between adjacent element pairs that are not explicitly checked for collisions as part of elementary tests between the nonadjacent pairs. Therefore, if we first check for collisions between the nonadjacent element pairs, we only need to perform elementary tests between the feature pairs that belong to O-Sets, and not all the feature pairs among adjacent elements.

Given an object, its O-Set is computed as part of a preprocess by analyzing the connectivity information among the volume meshes. A pseudocode description of construction algorithm for O-Set computation is given as Algorithm 3 in the Appendix.

*Incrementally updating the O-Sets.* As the model undergoes topology changes, the connectivity information changes. In this case, the O-Sets are incrementally updated to reflect the topology changes that can occur during splitting, tearing, or object breaking. For a volume object  $O'$  is generated from  $O$  with topology changes, it can be described as  $O' = O + A_s - A_t$ , where  $A_s$  is the set of volumetric elements that are added to  $O'$ ,  $A_t$  is the set of deleted volumetric elements from  $O$  that are no longer in  $O'$ . The O-Sets

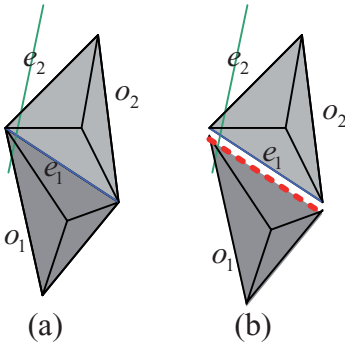


Fig. 9. Redundant elementary tests: The edge  $e_1$  is shared by two tetrahedra  $o_1$  and  $o_2$ . The edge  $e_1$  will be tested with another edge  $e_2$  twice, if  $o_1$  and  $o_2$  are tested with  $e_2$  independently.

are updated incrementally by removing feature pairs related to  $A_t$ , and adding new feature pairs in the proximity of  $A_s$ .

## 5.2 Assignment Culling

A large number of features (vertices, edges, and faces) are shared between volumetric elements. If we perform elementary tests between the volumetric element pairs independently, many redundant elementary tests are performed. This is illustrated in Figure 9(a).

These redundant tests can be eliminated using an assignment mechanism that ensures that a feature is assigned to only one volumetric element that is incident to the feature. As shown in Figure 9(b), the redundant EE test is removed by assigning  $e_1$  only to  $o_1$ .

The assignment mechanism has been used for triangle meshes [Curtis et al. 2008]. We extend this idea for volumetric elements as *static feature assignment*. The assignment is not unique as long as it satisfies the condition that a feature is assigned to a single volumetric element. A simple yet effective solution is to use a greedy algorithm to ensure that a feature is assigned to only one element (as shown in Algorithm 4 in the Appendix).

The main problem with static feature assignment is that it is not compatible with O-Sets. By using O-Sets, all the duplicate tests between adjacent volumetric elements are skipped. When using O-Sets with static feature assignment, some collisions between feature pairs may be missed when those feature pairs are assigned to adjacent volumetric elements. These feature pairs will be skipped when adjacent element pairs are skipped.

In order to overcome this problem, a nonadjacent constraint for the feature assignment is taken into account by the assignment scheme. We present this modification as the *dynamic feature assignment* method.

*Dynamic feature assignment.* For a feature pair  $\{elm1, elm2\}$  that is tested for CCD, we assign them in a dynamic manner. The pair  $\{elm1, elm2\}$  may be assigned to any volume elements among  $\{o_i, o_j\}$ , where  $o_i$  is incident to  $elm1$  and  $o_j$  is incident to  $elm2$ . There must be at least one element pair within  $\{o_i, o_j\}$  that  $o_i$  is not adjacent  $o_j$ . Otherwise  $\{elm1, elm2\}$  correspond to adjacent element pairs and will be proceeded by the O-Set computation algorithm. So we directly assign the pair  $\{elm1, elm2\}$  to the first nonadjacent volumetric element pair  $\{o_i, o_j\}$ . The dynamic feature assignment algorithm for a VF/EE test between a feature  $elm_1$  from  $o_1$  with another feature  $elm_2$  from  $o_2$  is performed in a similar manner. Also, we can use our culling method based on O-Sets without

any modification. A detailed pseudocode description is given in Algorithm 5 of the Appendix.

Another benefit of the dynamic assignment over the static assignment is that it naturally works for volume meshes with topology changes, since the feature assignment is performed during the run-time process. As new feature pairs are added or deleted, we change their assignment in a dynamic manner. This makes it possible to make our algorithm work well on scenes with topological changes.

## 6. IMPLEMENTATION AND PERFORMANCE

In this section, we describe our implementation and highlight the performance of our CCD algorithm on several benchmarks arising from engineering, medical, and animation simulations that have different characteristics.

### 6.1 Implementation

We have implemented a CCD system for volume meshes (VolCCD) based on our algorithm on a standard PC (Windows/XP 32 bits, Intel Q6600 CPU 2.4 GHz, 2GM RAM) by using C++. The timings are generated using a single thread running on a single core.

We compare the performance of our system (VolCCD), with the following two approaches.

- (1) *NavCCD*. This algorithm uses the k-DOP hierarchy, but performs all the elementary tests between the volumetric elements with overlapping bounding volumes. This way, we can evaluate the benefit of our culling schemes.
- (2) *HashCCD*. This algorithm is based on optimized spatial hashing [Teschner et al. 2003] as opposed to bounding volume hierarchies. Instead of discrete collision checks, we perform CCD between volume meshes using the elementary tests.

### 6.2 Benchmarks and Performance

In order to test the performance of our algorithm, we use 5 different benchmarks, arising from different simulations with different characteristics.

- (1) *Octopi*. Three deforming octopi with 24 tentacles contact with each other and generate a lot of inter-object and intra-object collisions (Figure 7).
- (2) *Bullet Penetration*. A high-speed copper bullet hits a steel target and achieves penetration (Figure 10). During the penetration, the topology changes result in a high number of interobject collisions.
- (3) *Airbag*. The deforming airbag has self-collisions as well as other collisions with the steering wheel (Figure 12).
- (4) *Car Crash*. A Ford Explorer crashes against a rigid wall and deforms (Figure 1). This benchmark is designed for car crash analysis.
- (5) *Cutting Liver*. A liver is cut during operation (Figure 13). This benchmark comes from surgery simulation.

Table I shows the average query time of VolCCD and the improvement over NavCCD and HashCCD, and culling ratios (the ratios of the number of elementary tests of VolCCD over the number of NavCCD), respectively. Overall our method shows more than one order of magnitude performance improvement over NavCCD and HashCCD across all the tested benchmarks. This overall performance improvement is mainly caused by the drastic reduction (about 100:1 reduction) of the tested number of elementary tests.

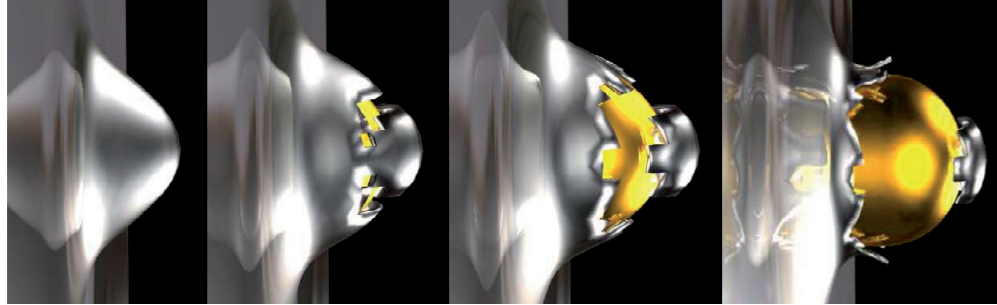


Fig. 10. Bullet penetration: A high-speed copper bullet (with 11.8 – 12K hexahedra) hits a steel target and results in topological changes.

Table I. Performance and Speedup

Model	Avg. Query	Speedup over NavCCD	Speedup over HashCCD	Culling ratio
Octopi	75ms	12x	18.3x	0.01%
Bullet	48ms	21x	28x	0.69%
Airbag	88ms	10.2x	13x	0.58%
Liver	53ms	10.3x	14.1x	0.72%
Ford	3.3s	12.4x	17.4x	3.54%

This table shows the average query time of VolCCD, performance improvements over NavCCD and HashCCD, and culling ratios (the ratios of the number of elementary tests of VolCCD over the number of NavCCD).

Table II. Culling Efficiency on the Octopi Benchmark

Culling	VF tests	EE tests	Total	Ratio
A	26M	312M	339M	100%
B	1.1M	6.4M	7.5M	2.23% (B/A)
C	7.9K	24K	32K	0.42% (C/B)

This table shows the number of VF and EE elementary tests performed for the deforming octopi benchmark without performing any culling (A), with feature-level culling only (B), and with element-level culling and feature-level culling (C). Each of them uses the 16-DOP BVH.

Table III. Culling Efficiency on the Car Crash Benchmark

Culling	VF tests	EE tests	Total	Ratio
A	8.24E + 09	1.6E + 10	2.43E + 10	100%
B	9.8E + 07	3.8E + 08	4.76E + 08	1.96% (B/A)
C	2.3E + 07	1.2E + 08	1.41E + 08	29.61% (C/B)

This table shows the number of VF and EE elementary tests performed for the benchmark Car Crash without performing any culling (A), with feature-level culling only (B), and with element-level and feature-level culling (C). Each of them uses the 16-DOP BVH.

Tables II and III highlight the efficiency of each culling technique. The culling ratio for the feature-level culling only is computed as a ratio of the number of elementary tests without any culling to that with the feature-level culling only. The culling ratio for the element-level culling and feature-culling is computed as a ratio of the number of elementary tests performed with both elementary-level and feature-culling to that with the feature-level culling only. In Table II, only 0.01% (= 2.23% \* 0.42%) tests of those passed culling have to be performed. In Table III, only 0.58% (= 1.96% \* 29.61%) tests of those passed culling have to be performed.

Figure 11 provides a breakdown of computational cost (computing k-DOPs, updating k-DOP-based BVH, BVH traversal and culling, and exact elementary tests) of our CCD method. For all the benchmarks, BVH updating and culling and exact elementary tests are the two most time-consuming steps (56% ~ 91%).

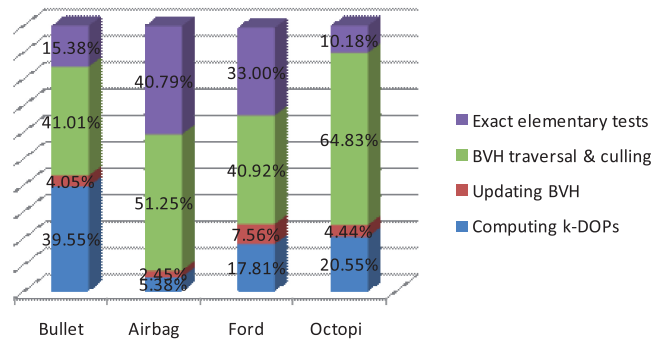


Fig. 11. Portions of the steps of our CCD algorithm: This figure provides a breakdown of computational cost of our CCD method (e.g., computing k-DOPs, updating k-DOP-based BVH, BVH traversal and culling, and exact elementary tests).

### 6.3 Continuous Trajectory with Topological Changes

In some benchmarks like the Cutting Liver and Bullet Penetration, the connectivity and topology changes. As a result, the number of vertices in the model may change and we cannot perform linear interpolation between the vertices. Instead, we use the previous position,  $p'$ , of a vertex  $p$  by subtracting its movement, that is,  $p' = p - s * v_p$ , where  $s$  is the simulation time step and  $v_p$  is the average velocity of  $p$  that is computed from the simulation. We perform linear interpolation between  $p$  and  $p'$ , and perform the CCD tests between them to compute the first time of contact.

## 7. ANALYSIS AND COMPARISON

In this section, we analyze the performance of our algorithm and compare its features with prior methods.

### 7.1 Analysis and Discussions

The performance improvement in our CCD algorithm for volume mesh comes from two factors: (1) significantly reducing the number of false positives based on CSAT tests and (2) eliminating redundant elementary tests based on the O-Sets and assignment culling.

The CSAT algorithm for a VF pair  $\{v, f\}$  only needs to perform 15 addition and 12 multiplication floating-point operations, when we use the normal vector of  $f$  as the separating axis. On the other hand, an exact elementary test between a VF pair takes roughly 155 addition, 217 multiplication, and 6 division operations, on average. As a result, the cost of the conservative CSAT culling method is about 6% to 8% of the total cost of the exact elementary test. Since

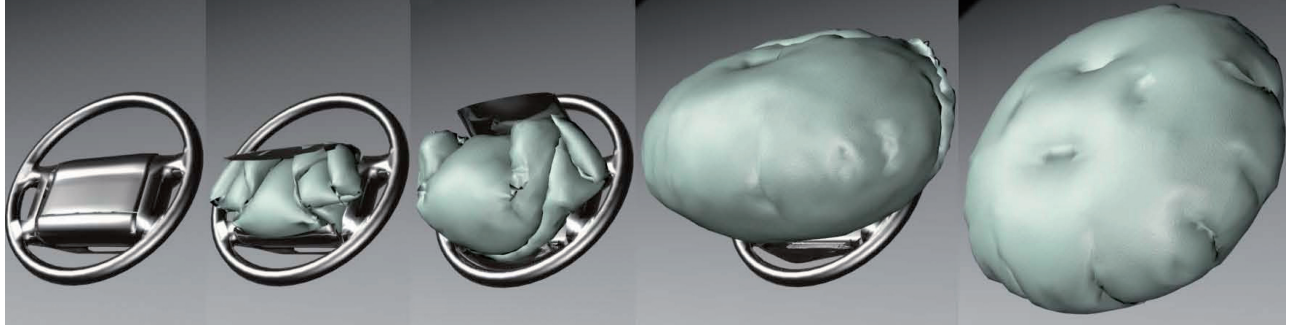


Fig. 12. Airbag: This deforming airbag has 9.1K shell elements. VolCCD performs inter-object and intra-object CCD queries at 88ms on average.

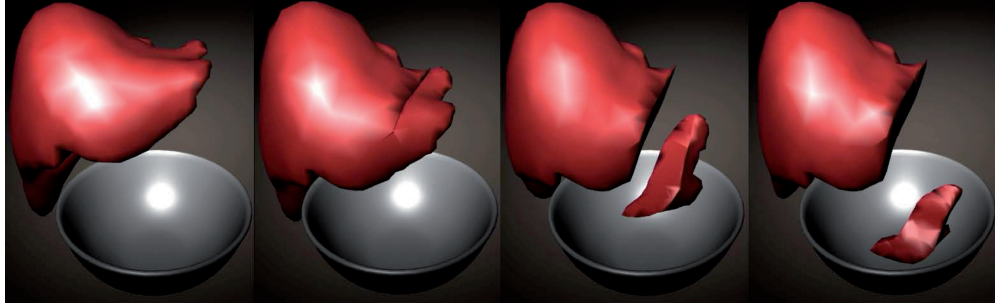


Fig. 13. Cutting liver: A liver is cut during a surgical operation. The model has 3874 tetrahedra initially and is deformed to have 4338 tetrahedra because of the cutting operation. The average CCD query time is 53.2ms per frame. We achieve more than 10 times improvement over prior methods.

the k-DOP hierarchy results in a high number of false positives, the CSAT culling method can be quite effective. Assignment culling is also effective in terms of removing redundant elementary tests between adjacent volumetric elements and nonadjacent volumetric elements with a very low overhead.

*Extension to nonconstant velocities.* Currently, our approach has been applied to deforming volumetric elements whose vertices have a constant velocity between the discrete instances. Note that the constant velocity assumption is widely used in many prior CCD algorithms (including surface-based algorithms), as mentioned in Section 3.1. It leads to a simple formulation to interpolate the motion between two discrete instances. In the case that the velocities of the vertices are not constant (e.g., the vertices are moving with acceleration  $a_i$ ), we have to use an appropriate function to model the trajectory of each vertex, as opposed to the linear trajectories shown in Figure 6. The CSAT culling method (Section 4) would be modified accordingly, but is still applicable. Since our approach is conservative, we expect that the culling efficiency would reduce in this case. If we model the motion using the constant acceleration, the resulting trajectory would correspond to quadratic polynomial functions of time  $t$ . The resulting elementary tests would involve computing the roots of degree 6 polynomials.

*Relative performance of surface-based vs. volume-based CCD algorithms.* Our method performs CCD to check for collisions that may occur on the surface boundary as well as among the internal volume elements. In some applications, only performing collision checking between surface-based boundary primitives may be sufficient. As a result, we compare the performance of a surface-based and volume-based algorithm. For the two cases (a) and (b) of the bullet penetration scene in Figure 3, the performance of volume-based collision detection is about 3.2X slower than the surface-based collision detection when running with a single thread. However, with

the help of SIMD instructions and multithreads (on a Intel Q6600 GPU with 4 cores), we observed that the volume-based method is just about 1.3X slower than the surface-based method by exploiting the parallelism.

*Collisions at the initial simulation time.* We have derived our culling method based on the assumption that there are no overlapping elements at the initial simulation time  $t = 0$ . However, our culling methods work even in this case, since our CCD algorithm reduces to discrete collision checking at  $t = 0$ .

## 7.2 Comparisons

In this section, we compare features of our algorithm with prior methods.

*Optimized spatial hashing.* Teschner et al. [2003] used optimized spatial hashing to accelerate discrete collision detection among deforming volume meshes. This method can be easily extended to perform CCD. We have also extended this method to HashCCD to perform CCD and tested it against our method. We can also combine our culling algorithms with it. However, in our benchmarks, we observed that k-DOP hierarchies offer much higher performance over spatial hashing, since some of our tested benchmarks have very dense geometry in localized regions.

*Flip methods.* Some researchers have advocated the use of flip methods to check for self-collisions among volume meshes, and these have been used for tetrahedral meshes [Erleben et al. 2005]. The flip method only checks whether a specific element of the mesh undergoes self-collision. It can be used as a sufficient condition to check for self-collisions, but it is not a necessary condition. In other words, even if there is no flip, self-collisions can also appear if we fail to resolve contacts among the surface boundary and thus have interpenetrations among the internal elements of the mesh.

*Normal cones.* Normal cones and continuous normal cones [Provot 1997; Tang et al. 2009] are used for self-collisions and work well on the portions of the boundaries that are relatively flat or have low variation in curvature. That approach is limited only to surface-based collision checking. In other words, it can only be applied to the boundary of the objects, and not to the interior elements. Since each volume mesh is a convex polytope, it is unclear whether normal cone culling can show meaningful culling.

*Orphan sets and representative triangles.* Orphan sets [Tang et al. 2009] and representative triangles [Curtis et al. 2008] are quite effective for removing redundant elementary tests between adjacent triangles and nonadjacent triangles of meshes. Our feature-level culling extends these ideas to volume meshes, and integrates them together with the dynamically assignment scheme.

*Image-space algorithms.* Many image-space algorithms that use GPU rasterization methods [Faure et al. 2008; Allard et al. 2010] can be used for interactive collision checking. However, the use of image-space methods can result in missed collisions, by using or relying on discrete image-space representations. Moreover, since different elements are connected to each other, it is unclear whether we can get a high culling ratio for volume meshes based on these image-space techniques.

*Coplanarity-based culling.* Our CSAT tests are complementary to coplanarity-based culling [Tang et al. 2010a]. Coplanarity-based culling checks for penetration along the interpolation trajectory of the deforming features. For example, to test a VF pair  $\{v, f\}$ , coplanarity-based culling computes the deforming normal vector  $n_t$  of a triangle, and tests the relative positions of  $v$  and  $f$  with respect to the plane defined by  $n_t$ . On the other hand, CSAT is used to check for separate directions and also extends to volumetric elements. Moreover, CSAT involves fewer arithmetic operations. In practice, for a single VF pair, the cost of CSAT is about two times lower than coplanarity-based culling. In terms of performing four VF pairwise tests between a tetrahedron and a vertex, CSAT is about six times faster than coplanarity-based culling.

*Continuous OBB test.* Redon et al. [2002], Levine [2000], and Eberly [2000] used continuous OBB tests to deal with (moving) rigid models. OBB trees are computed once for these models, and checked for overlap among objects undergoing rigid motion based on a “continuous OBB overlap test”. However, for deformable objects, OBBs may not be a good choice for bounding volume, as the updating cost is relatively high (15 ~ 25X slower) over k-DOPs. For example, the OBB overlap test includes about 180 operations: 15 comparisons, 60 add/sub, 81 mult, and 24 abs operations, which are much more expensive than our CSAT test. Therefore, we use k-DOPs because they provide a good balance between the culling efficiency and the updating cost.

### 7.3 Limitations

Our culling techniques have several limitations. The culling efficiency of assignment culling depends on the connectivity information between volumetric elements. Also, if there are high numbers of topological changes, then the cost of updating O-Set can be high. The efficiency and effectiveness of CSAT depends on the choice of the separating axis. Our current method uses a simple heuristic to estimate a good separating axis, and it may not work well in all cases. The CSAT culling algorithm has an additional overhead. If the number of false positives after the BVH culling is relatively low, the use of the CSAT culling algorithm can result in reduced performance, although the slowdown would be minor because of the small overhead of the CSAT culling method. Also, in some simulations where we do not have strong external forces, contacts

occurred in constrained geometric configurations, or high impacts with fast moving objects, detecting contacts based only on the surface boundary may be sufficient to generate realistic results.

## 8. CONCLUSION AND FUTURE WORK

We have presented a novel algorithm for CCD between volume meshes. Our BVH-based approach is applicable to the contact handling of various kinds of volumetric elements that is needed in different FEM applications, physically-based simulation, engineering analysis, and medical applications. Moreover, our CCD algorithms accurately compute the first time of contact and hereby make it possible to use a larger simulation time step while providing a high-quality contact information. We have highlighted its performance on many benchmarks and observed more than an order of magnitude performance improvement. To the best of our knowledge, VolCCD is the first interactive algorithm that can perform accurate collision checking for FEM or other simulations that use a few thousands to hundreds of thousands of tetrahedra or triangular prisms.

There are many avenues for future work. In addition to addressing the limitations of our method mentioned before, we would like to improve the performance of our method by employing multiple CPU cores or GPUs [Tang et al. 2011]. We expect that all the proposed culling methods map very well with parallel implementation. Even though we have drastically reduced the number of false positives, we still perform a high number of elementary tests for complex benchmarks, such as car crash simulation composed of 1.2M shells. We would like to design exact and less conservative culling methods to improve the performance of our method. Finally, we would also like to integrate our algorithm with FEM simulators and design interactive simulation techniques.

## APPENDIXES

### Proof of Theorem and Corollaries

**THEOREM 1 (CSAT FOR TWO MOVING VERTICES).** Suppose two moving vertices  $p$  and  $q$ , defined by their positions at the time interval  $[0, 1]$  ( $p_0$  and  $p_1$  and  $q_0$  and  $q_1$ , respectively), and a separating axis defined by  $\mathbf{L} (\neq 0)$ . If  $(q_0 - p_0) \cdot \mathbf{L}$  and  $(q_1 - p_1) \cdot \mathbf{L}$  have the same sign,  $q$  will not overlap with  $p$  during the time interval.

**PROOF.** We define  $\mathbf{v}_q$  and  $\mathbf{v}_p$  as  $\mathbf{v}_q = q_1 - q_0$  and  $\mathbf{v}_p = p_1 - p_0$  respectively. We also let  $\mathbf{L}'$  be the normalized vector of the  $\mathbf{L}$ , that is,  $\mathbf{L}' = \frac{\mathbf{L}}{\|\mathbf{L}\|}$ .

Then the projected distance of  $q$  and  $p$  along  $\mathbf{L}$ ,  $d_{pq}$ , is given as

$$\begin{aligned} d_{qp} &= (q - p) \cdot \mathbf{L}' \\ &= [(q_0 - p_0) + t * (\mathbf{v}_q - \mathbf{v}_p)] \cdot \mathbf{L}' \\ &= \frac{(q_0 - p_0) \cdot \mathbf{L} + t * (\mathbf{v}_q - \mathbf{v}_p) \cdot \mathbf{L}}{\|\mathbf{L}\|}, \end{aligned} \quad (5)$$

where  $t$  is a time parameter and  $t \in [0, 1]$ . As a result,  $d_{pq}$  is within a bound as follows

$$d_{pq} \in \left[ \frac{(q_0 - p_0) \cdot \mathbf{L}}{\|\mathbf{L}\|}, \frac{(q_0 - p_0) \cdot \mathbf{L} + (\mathbf{v}_q - \mathbf{v}_p) \cdot \mathbf{L}}{\|\mathbf{L}\|} \right] \quad (6)$$

This is equivalent to

$$d_{pq} \in \left[ \frac{(q_0 - p_0) \cdot \mathbf{L}}{\|\mathbf{L}\|}, \frac{(q_1 - p_1) \cdot \mathbf{L}}{\|\mathbf{L}\|} \right]. \quad (7)$$

Since  $(q_0 - p_0) \cdot \mathbf{L}$  and  $(q_1 - p_1) \cdot \mathbf{L}$  have the same sign,  $d_{pq}$  will not be zero. This implies that the projections of  $q$  and  $p$  on  $\mathbf{L}$  are disjoint, and thus  $q$  and  $p$  do not overlap.  $\square$

**COROLLARY 1 (CSAT BETWEEN A VERTEX AND A TRIANGLE).** Suppose a vertex  $p$  and a triangle  $f$  defined by their positions at the time interval  $[0, 1]$  ( $p_0$  and  $p_1$  for  $p$ , and  $a_0, b_0, c_0$  and  $a_1, b_1, c_1$  for  $f$ , respectively), and a vector  $\mathbf{L}$  ( $\neq 0$ ). If the following 6 expressions have the same sign:

$$\begin{aligned} (a_0 - p_0) \cdot \mathbf{L}, & \quad (a_1 - p_1) \cdot \mathbf{L}, & \quad (b_0 - p_0) \cdot \mathbf{L}, \\ (b_1 - p_1) \cdot \mathbf{L}, & \quad (c_0 - p_0) \cdot \mathbf{L}, & \quad (c_1 - p_1) \cdot \mathbf{L}, \end{aligned} \quad (8)$$

then  $p$  and  $f$  will not overlap during the time interval.

**PROOF.** Let  $q$  be a point inside  $f$ , and it can be expressed as a convex combination of  $a, b, c$ , that is,  $q = u * a + v * b + w * c$ . Here,  $u, v, w \in [0, 1]$ , and  $u + v + w = 1$ . The projected distance of  $p$  and  $q$  along  $\mathbf{L}$  is given as

$$\begin{aligned} d_{qp} &= (q - p) \cdot \mathbf{L}' = (u * a + v * b + w * c - p) \cdot \mathbf{L}' \\ &= (u * (a - p) + v * (b - p) + w * (c - p)) \cdot \mathbf{L}'. \end{aligned}$$

We build on CSAT for two vertices. Since all the scalar values in Eq. (8) have the same sign,  $(a - p) \cdot \mathbf{L}', (b - p) \cdot \mathbf{L}',$  and  $(c - p) \cdot \mathbf{L}'$  will have the same sign as well. Therefore,  $d_{qp}$  will not be zero. It means that  $p$  and  $f$  will not overlap during the time interval.  $\square$

**COROLLARY 2 (CSAT BETWEEN A VERTEX AND A VOLUMETRIC ELEMENT).** Suppose a vertex  $p$  and a volumetric element  $o$  (with  $n_v$  vertices and  $n_f$  triangles) defined by their positions during the time interval  $[0, 1]$  ( $p_0$  and  $p_1$  for  $p$ , and  $q_0^i$  and  $q_1^i$  for  $o$ ,  $i \in [0, n_v - 1]$ ), and a vector  $\mathbf{L}$  ( $\neq 0$ ). If the following  $2 * n_v$  algebraic expressions have the same sign:

$$\begin{aligned} (q_0^i - p_0) \cdot \mathbf{L}, & \quad i \in [0, n_v - 1], \\ (q_1^i - p_1) \cdot \mathbf{L}, & \quad i \in [0, n_v - 1], \end{aligned} \quad (9)$$

then  $p$  and all the  $n_f$  triangles of  $o$  will not overlap during the time interval.

**PROOF.** Since all of  $n_f$  triangles are defined by these  $n_v$  vertices, all the scalar values in Eq. (8) have the same sign for all the triangles of  $o$ . As a result, all the VF tests corresponding to different triangles of  $o$  can be culled away.  $\square$

**COROLLARY 3 (CSAT BETWEEN TWO EDGES).** Suppose two edges,  $e^1$  and  $e^2$ , defined by their end positions during  $t \in [0, 1]$  ( $a_0, b_0$  and  $a_1, b_1$  for  $e^1$ , and  $c_0, d_0$  and  $c_1, d_1$  for  $e^2$ ), and a vector  $\mathbf{L}$  ( $\neq 0$ ). If the following eight expressions have the same sign:

$$\begin{aligned} (a_0 - c_0) \cdot \mathbf{L}, (a_1 - c_1) \cdot \mathbf{L}, (b_0 - c_0) \cdot \mathbf{L}, (b_1 - c_1) \cdot \mathbf{L}, \\ (a_0 - d_0) \cdot \mathbf{L}, (a_1 - d_1) \cdot \mathbf{L}, (b_0 - d_0) \cdot \mathbf{L}, (b_1 - d_1) \cdot \mathbf{L}, \end{aligned} \quad (10)$$

then  $e^1$  and  $e^2$  do not overlap during the time interval.

**PROOF.** Based on CSAT for two vertices, if the first four expressions have the same sign then the projections of  $a$  and  $b$  are below/above the projection of  $c$  along  $\mathbf{L}$ . If the last four expressions have the same sign, then the projections of  $a$  and  $b$  are below/above the projection of  $d$  along  $\mathbf{L}$ . All the points on  $e^1, e_i^1$ , can be expressed as a convex combination of  $a$  and  $b$ . Similarly, all the points on  $e^2, e_i^2$ , can be expressed as a convex combination of  $c$  and  $d$ . So the projection of  $e_i^1$  is below/above the projection of  $e_i^2$ . If their projections on the axis do not overlap, we can conclude that the original edges will not overlap.  $\square$

**COROLLARY 4 (CSAT BETWEEN AN EDGE AND A VOLUMETRIC ELEMENT).** Suppose an edge  $e$  and a volumetric element  $o$  (with  $n_v$

---

**ALGORITHM 2:** CSAT culling between two volumetric elements  $o_i$  and  $o_j$ .

---

```

1: for all vertex  $v_1 \in o_i$  do
2:   Perform CSAT culling between  $v_1$  and  $o_j$  with Corollary 2
3: end for
4: for all vertex  $v_2 \in o_j$  do
5:   Perform CSAT culling between  $v_2$  and  $o_i$  with Corollary 2
6: end for
7: for all edge  $e_1 \in o_j$  do
8:   Perform CSAT culling between  $e_1$  and  $o_i$  with Corollary 4
9: end for

```

---

vertices and  $n_e$  edges) defined by their positions at time interval  $[0, 1]$  ( $c_0$  and  $c_1$  and  $d_0$  and  $d_1$  for  $e$ , and  $q_0^i$  and  $q_1^i$  for  $o$ ,  $i \in [0, n_v - 1]$ ), and a vector  $\mathbf{L}$  ( $\neq 0$ ). If the following  $4 * n_v$  expressions have the same sign:

$$\begin{aligned} (q_0^i - c_0) \cdot \mathbf{L}, i \in [0, n_v - 1], (q_1^i - c_1) \cdot \mathbf{L}, i \in [0, n_v - 1], \\ (q_0^i - d_0) \cdot \mathbf{L}, i \in [0, n_v - 1], (q_1^i - d_1) \cdot \mathbf{L}, i \in [0, n_v - 1], \end{aligned} \quad (11)$$

then  $e$  and  $o$  do not overlap during the time interval.

**PROOF.** Since all the  $n_e$  edges are defined by these  $n_v$  vertices, the Eq. (10) holds for all these edges. As a result, all the EE pairs between  $e$  and  $o$  are culled away.  $\square$

## Algorithms

The pseudocode for performing CSAT culling between two volumetric elements,  $o_i$  and  $o_j$ , is shown as Algorithm 2. It is executed as 3 stages. We first perform CSAT culling between every vertex  $v_1 \in o_i$  with  $o_j$ , then perform CSAT culling between every vertex  $v_2 \in o_j$  with  $o_i$ , finally perform CSAT culling between every edge  $e_1 \in o_j$  with  $o_i$ .

The O-Set is constructed by using Algorithm 3. In this algorithm, all the adjacent volumetric element pairs are traversed. For each one of these pairs  $\{o_i, o_j\}$ , we check all the feature pairs  $\{elm_1, elm_2\}$ , here  $elm_1 \in o_i$  &  $elm_2 \in o_j$ . If one of the volumetric elements in the incident set of  $elm_1, o_k$ , is not adjacent to  $o_j$ , then the feature pair  $\{elm_1, elm_2\}$  is checked based on testing a nonadjacent element pair  $\{o_k, o_j\}$ . As a result, we do not need to store  $\{elm_1, elm_2\}$  in the O-Set. Similarly, if one of the volumetric elements in the incident set of  $elm_2, o_l$ , is not adjacent to  $o_i$ , then the feature pair  $\{elm_1, elm_2\}$  is checked for collision while handling the nonadjacent element pair  $\{o_l, o_i\}$ . As a result, we do not include the pair in the O-Set. Otherwise, the feature pair  $\{elm_1, elm_2\}$  is inserted in the O-Set.

Algorithm 4 highlights the details of static feature assignment computation. A greedy approach is used by traversing all the volumetric elements. For each volumetric element  $o_i$ , we check its features. For each feature  $elm_j$  of  $o_i$ , if it has not been assigned to any volume element, then it is assigned to  $o_i$ .

Algorithm 5 shows the details of the dynamic feature assignment algorithm. The dynamic feature assignment is performed before we perform an exact elementary test for a feature pair  $\{elm_1, elm_2\}$ , where  $elm_1$  belongs to  $o_1$  and  $elm_2$  belongs to  $o_2$ . We traverse each element pair  $\{o_i, o_j\}$ , where  $o_i$  is incident to  $elm_1$ , and  $o_j$  is incident to  $elm_2$ . In the case that  $o_i$  is not adjacent to  $o_j$ , we perform the exact test between  $elm_1$  and  $elm_2$  only if  $o_i = o_1$  and  $o_j = o_2$ .

**ALGORITHM 3:** O-Set Construction: Compute the O-Set based on connectivity information.

---

```

1: for all adjacent element pair  $\{o_i, o_j\}$  do
2:   for all feature pair  $\{elm_1 \in o_i, elm_2 \in o_j\}$  do
3:     for all elements  $o_k \in$  the incident set of  $elm_1$  do
4:       if  $o_k$  is not adjacent to  $o_j$  then
5:         return
6:       end if
7:     end for
8:     for all elements  $o_l \in$  the incident set of  $elm_2$  do
9:       if  $o_l$  is not adjacent to  $o_i$  then
10:        return
11:      end if
12:    end for
13:  end for
14:  add  $\{elm_1, elm_2\}$  into O-Set
15: end for
```

---

**ALGORITHM 4:** Static Feature Assignment: Assign each feature to and only to a volumetric element.

---

```

1: for all volumetric elements  $o_i$  do
2:   for all feature  $elm_j \in o_i$  do
3:     if  $elm_j$  has not been assigned then
4:       assign  $elm_j$  to  $o_i$ 
5:     end if
6:   end for
7: end for
```

---

**ALGORITHM 5:** Dynamic Feature Assignment: assignment for a test between a feature  $elm_1$  from  $o_1$  and another feature  $elm_2$  from  $o_2$ .

---

```

1: for all volumetric elements  $o_i \in$  the incident set of  $elm_1$  do
2:   for all volumetric elements  $o_j \in$  the incident set of  $elm_2$  do
3:     if  $o_i$  is not adjacent to  $o_j$  then
4:       if  $o_i = o_1$  AND  $o_j = o_2$  then
5:         ElementaryTest( $elm_1, elm_2$ )
6:       else
7:         return
8:       end if
9:     end if
10:   end for
11: end for
```

---

#### ACKNOWLEDGMENTS

We would like to thank Jeremie Allard and SOFA team for providing Octopi Benchmark [Allard et al. 2010] and Liver Cutting Benchmark, and helping us with the rendering. We thank Miguel Otaduy for useful discussions and thoughtful comments on an earlier draft. The Car Crash Benchmark and Airbag benchmarks from the Finite Element Model Archive were provided by NCAC [National-Crash-Analysis-Center 2010]. We also want to thank Daniel Heiserer from BMW for many useful discussions.

#### REFERENCES

- ABAQUS. 2003. *ABAQUS 6.4. Analysis User's Manual*. Hibbit, Karlsson & Sorensen, Inc.
- ALLARD, J., FAURE, F., COURTECUISSE, H., FALIPOU, F., DURIEZ, C., AND KRY, P. G. 2010. Volume contact constraints at arbitrary resolution. In *Proceedings of the ACM SIGGRAPH Conference*. ACM, 1–10.
- BRIDSON, R., FEDIKIW, R., AND ANDERSON, J. 2002. Robust treatment of collisions, contact and friction for cloth animation. *ACM Trans. Graph.* 21, 3, 594–603.
- CURTIS, S., TAMSTORF, R., AND MANOCHA, D. 2008. Fast collision detection for deformable models using representative-triangles. In *Proceedings of the Symposium on Interactive 3D Graphics and Games*. 61–69.
- EBERLY, D. H. 2000. *3D Game Engine Design: A Practical Approach to Real-Time Computer Graphics*. Morgan Kaufmann.
- ERLEBEN, K., DOHLMANN, H., AND SPORRING, J. 2005. The adaptive thin shell tetrahedral mesh. In *J. WSCG*. 17–24.
- FAURE, F., BARBIER, S., ALLARD, J., AND FALIPOU, F. 2008. Image-based collision detection and response between arbitrary volume objects. In *Proceedings of the Symposium on Computer Animation*. 155–162.
- FISHER, S. AND LIN, M. C. 2001. Deformed distance fields for simulation of non-penetrating flexible bodies. In *Proceedings of the Eurographic Workshop on Computer Animation and Simulation*. Springer, 99–111.
- FLEISSNER, F., EBERHARD, P., BISCHOF, C., BRÜCKER, M., GIBBON, P., JOUBERT, G. R., MOHR, B., (EDS., F. P., FLEISSNER, F., AND EBERHARD, P. 2007. Load balanced parallel simulation of particle-fluid dem-sph systems with moving boundaries. In *Proceedings of Parallel Computing: Architectures, Algorithms and Applications Conference*. 37–44.
- GOTTSCHALK, S., LIN, M., AND MANOCHA, D. 1996. OBB-Tree: A hierarchical structure for rapid interference detection. In *Proceedings of ACM Siggraph Conference*. 171–180.
- GOVINDARAJU, N., KNOTT, D., JAIN, N., KABUL, I., TAMSTORF, R., GAYLE, R., LIN, M., AND MANOCHA, D. 2005. Interactive collision detection between deformable models using chromatic decomposition. *ACM Trans. Graph.* 24, 3, 991–999.
- HALLQUIST, J. 2006. LS-DYNA Theory Manual. Livermore Software Technology Corporation.
- HEIDELBERGER, B., TESCHNER, M., AND GROSS, M. 2003. Real-time volumetric intersections of deforming objects. In *Proceedings of Vision Modeling Visualization Conference (VMV'03)*. 461–468.
- HEIDELBERGER, B., TESCHNER, M., KEISER, R., MÜLLER, M., AND GROSS, M. 2004. Consistent penetration depth estimation for deformable collision response. In *Proceedings of Vision Modeling Visualization Conference (VMV'04)*. 330–346.
- HEO, J.-P., SEONG, J.-K., KIM, D., OTADUY, M. A., HONG, J.-M., TANG, M., AND YOON, S.-E. 2010. FASTCD: Fracturing-Aware stable collision detection. In *Proceedings of the ACM SIGGRAPH / Eurographics Symposium on Computer Animation*.
- HUTTER, M. AND FUHRMANN, A. 2007. Optimized continuous collision detection for deformable triangle meshes. In *Proceedings of the WSCG '07*. 25–32.
- IRVING, G., TERAN, J., AND FEDIKIW, R. 2004. Invertible finite elements for robust simulation of large deformation. In *Proceedings of the Symposium on Computer Animation*. 131–140.
- KŁOSOWSKI, J., HELD, M., MITCHELL, J., SOWIZRAL, H., AND ZIKAN, K. 1998. Efficient collision detection using bounding volume hierarchies of k-dops. *IEEE Trans. Vis. Comput. Graph.* 4, 1, 21–37.
- LEVINE, R. 2000. Collisions of moving objects. [http://realtimecollisions.com/files/levine\\_swept\\_sat.txt](http://realtimecollisions.com/files/levine_swept_sat.txt).

- LOMBARDO, J.-C., PAULE CANI, M., AND NEYRET, F. 1999. Real-time collision detection for virtual surgery. In *Proceedings of the Symposium on Computer Animation*. 26–28.
- LS-DYNA. 2001. Contact modeling in LS-DYNA. <http://www.dynasupport.com/tutorial/contact-modeling-in-ls-dyna/contact-types>.
- MATHIAS, E. AND GU, L. 2007. Hierarchical spatial hashing for real-time collision detection. In *Proceedings of the IEEE International Conference on Shape Modeling and Applications*. 61–70.
- MÜLLER, M., McMILLAN, L., DORSEY, J., AND JAGNOW, R. 2001. Real-time simulation of deformation and fracture of stiff materials. In *Proceedings of the Eurographic Workshop on Computer Animation and Simulation*. 113–124.
- NATIONAL-CRASH-ANALYSIS-CENTER. 2010. Finite element model archive. <http://www.ncac.gwu.edu/vml/models.html>.
- NEALEN, A., MÜLLER, M., KEISER, R., BOXERMAN, E., AND CARLSON, M. 2006. Physically based deformable models in computer graphics. *Comput. Graph. Forum* 25, 4, 809–836.
- O'BRIEN, J. F. 2000. Graphical modeling and animation of brittle fracture. Ph.D. thesis, Georgia Institute of Technology, Atlanta, GA.
- O'BRIEN, J. F. AND HODGINS, J. K. 1999. Graphical modeling and animation of brittle fracture. In *Proceedings of the 26th Annual Conference on Computer Graphics and Interactive Techniques*. 137–146.
- PARKER, E. G. AND O'BRIEN, J. F. 2009. Real-Time deformation and fracture in a game environment. In *Proceedings of the Symposium on Computer Animation*. 165–175.
- PLIMPTON, S., ATTAWAY, S., HENDRICKSON, B., SWEGLE, J., VAUGHAN, C., AND GARDNER, D. 1998. Parallel transient dynamics simulations: Algorithms for contact detection and smoothed particle hydrodynamics. *J. Parallel Distrib. Comput.* 50, 1-2, 104–122.
- PROVOT, X. 1997. Collision and self-collision handling in cloth model dedicated to design garment. In *Proceedings of the Graph. Interface Conference*. 177–189.
- REDON, S., KHEDDAR, A., AND COQUILLART, S. 2002. Fast continuous collision detection between rigid bodies. *Comput. Graph. Forum* 21, 3, 279–288.
- SIFAKIS, E., DER, K. G., AND FEDIKIW, R. 2007. Arbitrary cutting of deformable tetrahedralized objects. In *Proceedings of the ACM SIGGRAPH/Eurographics Symposium on Computer Animation*. 73–80.
- SUD, A., GOVINDARAJU, N., GAYLE, R., KABUL, I., AND MANOCHA, D. 2006. Fast proximity computation among deformable models using discrete voronoi diagrams. In *Proceedings of the ACM SIGGRAPH Conference*. 1144–1153.
- TANG, M., CURTIS, S., YOON, S.-E., AND MANOCHA, D. 2009. ICCD: Interactive continuous collision detection between deformable models using connectivity-based culling. *IEEE Trans. Vis. Comput. Graph.* 15, 4, 544–557.
- TANG, M., KIM, Y. J., AND MANOCHA, D. 2010b. Continuous collision detection for non-rigid contact computations using local advancement. In *Proceedings of International Conference on Robotics and Automation*.
- TANG, M., MANOCHA, D., LIN, J., AND TONG, R. 2011. Collision-streams: Fast GPU-based collision detection for deformable models. In *Proceedings of the ACM SIGGRAPH Symposium on Interactive 3D Graphics and Games (I3D'11)*. 63–70.
- TANG, M., MANOCHA, D., AND TONG, R. 2010a. Fast continuous collision detection using deforming non-penetration filters. In *Proceedings of the ACM SIGGRAPH Symposium on Interactive 3D Graphics and Games (I3D'10)*. ACM, New York, 7–13.
- TESCHNER, M., HEIDELBERGER, B., MÜLLER, M., POMERANETS, D., AND GROSS, M. 2003. Optimized spatial hashing for collision detection of deformable objects. In *Proceedings of Vision Modeling Visualization Conference (VMV'03)*. 47–54.
- TESCHNER, M., KIMMERLE, S., HEIDELBERGER, B., ZACHMANN, G., RAGHUPATHI, L., FUHRMANN, A., CANI, M.-P., FAURE, F., MAGNENAT-THALMANN, N., STRASSER, W., AND VOLINO, P. 2005. Collision detection for deformable objects. *Comput. Graph. Forum* 19, 1, 61–81.
- VOLINO, P. AND MAGNENAT-THALMANN, N. 2006. Resolving surface collisions through intersection contour minimization. *ACM Trans. Graph.* 25, 3, 1154–1159.
- VOLINO, P. AND THALMANN, N. M. 1994. Efficient self-collision detection on smoothly discretized surface animations using geometrical shape regularity. *Comput. Graph. Forum* 13, 3, 155–166.
- WOJTAN, C., THÜREY, N., GROSS, M., AND TURK, G. 2009. Deforming meshes that split and merge. *ACM Trans. Graph.* 28, 76:1–76:10.
- ZHANG, X., REDON, S., LEE, M., AND KIM, Y. J. 2007. Continuous collision detection for articulated models using taylor models and temporal culling. *ACM Trans. Graph.* 26, 3, 15.
- ZHU, Y., SIFAKIS, E., TERAN, J., AND BRANDT, A. 2010. An efficient multigrid method for the simulation of high-resolution elastic solids. *ACM Trans. Graph.* 29, 2, 1–18.

Received August 2010; revised January 2011; accepted June 2011